Germline Maintenance Through the Multifaceted Activities of GLH/Vasa in *Caenorhabditis elegans* P Granules

Elisabeth A. Marnik,* J. Heath Fuqua,*,† Catherine S. Sharp,* Jesse D. Rochester,*,‡ Emily L. Xu,*,§ Sarah E. Holbrook,*,‡, and Dustin L. Updike*,1**

*The Mount Desert Island Biological Laboratory, Bar Harbor, Maine 04672, †The College of the Atlantic, Bar Harbor, Maine 04609, ‡Graduate School of Biomedical Science and Engineering, University of Maine, Orono, Maine 04469, §The College of William and Mary, Williamsburg, Virginia 23185, and **The Jackson Laboratory, Bar Harbor, Maine 04609

ORCID IDs: 0000-0002-5199-6835 (E.A.M.); 0000-0002-1745-3669 (D.L.U.)

ABSTRACT Vasa homologs are ATP-dependent DEAD-box helicases, multipotency factors, and critical components that specify and protect the germline. They regulate translation, amplify piwi-interacting RNAs (piRNAs), and act as RNA solvents; however, the limited availability of mutagenesis-derived alleles and their wide range of phenotypes have complicated their analysis. Now, with clustered regularly interspaced short palindromic repeats (CRISPR/Cas9), these limitations can be mitigated to determine why protein domains have been lost or retained throughout evolution. Here, we define the functional motifs of GLH-1/Vasa in *Caenorhabditis elegans* using 28 endogenous, mutant alleles. We show that GLH-1's helicase activity is required to retain its association with P granules. GLH-1 remains in P granules when changes are made outside of the helicase and flanking domains, but fertility is still compromised. Removal of the glycine-rich repeats from GLH proteins progressively diminishes P-granule wetting-like interactions at the nuclear periphery. Mass spectrometry of GLH-1-associated proteins implies conservation of a transient piRNA-amplifying complex, and reveals a novel affinity between GLH-1 and three structurally conserved PCI (26S Proteasome Lid, COP9, and eIF3) complexes or "zomes," along with a reciprocal aversion for assembled ribosomes and the 26S proteasome. These results suggest that P granules compartmentalize the cytoplasm to exclude large protein assemblies, effectively shielding associated transcripts from translation and associated proteins from turnover. Within germ granules, Vasa homologs may act as solvents, ensuring mRNA accessibility by small RNA surveillance and amplification pathways, and facilitating mRNA export through germ granules to initiate translation.

KEYWORDS Vasa; GLH-1; DDX4; germ granules; P granules; *C. elegans*; germline; PCI complex

Germ cells and somatic cells from an individual carry identical copies of DNA, yet only germ cells have the potential to give rise to all the cell types of each subsequent generation. This suggests that epigenetic factors confer a germ cell's totipotent and immortal potential. These epigenetic factors are not limited to chromatin modifications, but also reside in the germ cell cytoplasm, or germ plasm. In some cases, the presence of germ plasm alone has been sufficient to reprogram somatic nuclei to restore cellular potency and immortal potential [reviewed in Strome and Updike (2015)]. Germ plasm contains a heterogeneous mix of RNA and protein that is not expressed in differentiating somatic tissue. In some animals, these germ cell-specific ribonucleoproteins phase separate in the cytoplasm to form what are called germ granules [reviewed in Marnik and Updike (2019)]. Depletion of germ granules in *Caenorhabditis elegans* causes sterility and germ-to-soma transformation, suggesting that they contain the cytoplasmic components that preserve germ cell totipotency (Updike *et al.* 2014; Knutson *et al.* 2017). A conserved protein that is consistently observed in the germ plasm and germ granules across species is collectively known as Vasa. Vasa and its homologs are required for germline specification, and have been shown more recently to influence somatic multipotency during development, regeneration,

doi: https://doi.org/10.1534/genetics.119.302670
Manuscript received August 7, 2019; accepted for publication September 3, 2019; published Early Online September 10, 2019.
Available freely online through the author-supported open access option.
Supplemental material available at FigShare: https://doi.org/10.25386/genetics.9497666.
[1]Corresponding author: The Mount Desert Island Biological Laboratory, 159 Old Bar Harbor Road, Salisbury Cove, ME 04672. E-mail: dupdike@mdibl.org

and tumorigenesis [reviewed in Poon *et al.* (2016)]. Therefore, understanding Vasa's molecular function and its complex role as a multipotency factor is critical.

Vasa was cloned in *Drosophila* just over 30 years ago as a DEAD-box helicase with homology to the eukaryotic initiation factor-4A (eIF4A) (Hay *et al.* 1988; Lasko and Ashburner 1988) and a binding partner to the translation initiation factor (eIF5B) (Carrera *et al.* 2000). These findings strongly suggested that Vasa and its homologs function to initiate and/or regulate translation in the germline, which was subsequently demonstrated by the eIF5B-dependent accumulation of *Gurken* and *mei-P26* in *Drosophila* (Johnstone and Lasko 2004; Liu *et al.* 2009). A more recent focus has been on Vasa's RNA-independent interactions with Argonaute proteins through a transient amplifying complex that impacts ping-pong-mediated piwi-interacting RNA (piRNA) amplification (Megosh *et al.* 2006; Malone *et al.* 2009; Kuramochi-Miyagawa *et al.* 2010; Xiol *et al.* 2014; Dehghani and Lasko 2016; Wenda *et al.* 2017). Other studies have demonstrated the ability of Vasa homologs (*i.e.*, DDX4) to form phase-separated organelles in cell culture that melt nucleic acid duplexes and act as a solvent for single-stranded RNA (Nott *et al.* 2015, 2016). The roles of Vasa homologs in translational regulation, piRNA amplification, and as an mRNA solvent demonstrate the protein's diversity of functions within the germline [reviewed in Lasko (2013)].

Phenotypes of various mutant Vasa alleles in *Drosophila* reflect this diversity of function. Strong alleles exhibit recessive female sterility in homozygotes due to defective oocyte development. Moderate Vasa alleles produce oocytes, but after fertilization the resulting embryos arrest with posterior patterning defects and no germ cells. Mutants rescued with a Vasa transgene carrying weak alleles permit some embryos to hatch and develop into adults that exhibit a range of fertility defects (Dehghani and Lasko 2015). Vasa phenotypes are also diverse across organisms. For example, Vasa mutations in *Drosophila* cause female-specific sterility whereas mutations in the Vasa homolog DDX4 cause male-specific sterility in mice (Wenda *et al.* 2017). Furthermore, while Vasa is conserved across metazoans, some animals such as *C. elegans* amplify piRNA silencing through RNA-dependent RNA polymerases (RdRPs) instead of the ping-pong method used by insects and mammals that lack RdRPs. Because of these differences, a comparative analysis of Vasa in different organisms is needed to determine conserved and divergent functions of germline maintenance, and specification.

The comparison of Vasa function in model organisms has traditionally been limited by available mutants, making it difficult or impossible to gain insight on structural motifs from available alleles exhibiting a wide range of phenotypes. This was especially true in *C. elegans*, where the function of one of its Vasa homologs, GLH-1, could only be inferred from a small handful of alleles that still made truncated proteins (Spike *et al.* 2008). However, with the advent of CRISPR technology, it has become possible to make modifications to endogenous genes to replicate informative alleles in conserved residues. Using this approach, over two dozen site-directed mutant alleles of *glh-1* were created in a strain where the endogenous gene carried a C-terminal GFP::3xFLAG fusion. Each modification was then examined to determine its influence on fertility and embryonic viability, in the context of its effect on GLH-1 expression and distribution in the embryonic and adult germline. These results emphasize the role of GLH-1's helicase activity in maintaining P granule association and provide insight into the functional domains that distinguish Vasa proteins from the dozens of other DEAD-box helicases encoded in the *C. elegans* genome.

Vasa protein interactions may be very transient, making them difficult to detect. Previous DEAD-box helicase studies have utilized mutations within the DEAD motif that are thought to either inhibit substrate binding or lock in bound substrates, with the idea of capturing different interaction partners at distinctive, and often transient, enzymatic steps (Pause and Sonenberg 1992; Cruciat *et al.* 2013; Xiol *et al.* 2014; Yang *et al.* 2014). In this report, immunoprecipitation (IP) liquid chromatography (LC)-mass spectrometry (MS)/MS was used to identify proteins with increased GLH-1 association, and examine what happens to those associations in the substrate-inhibited or locked states. These results suggest that GLH-1 associates with evolutionarily conserved PCI (26S Proteasome Lid, COP9 signalosome, and eIF3) scaffolding complexes or zomes to regulate protein translation and degradation. In the locked state, GLH-1 shows increased affinity for a handful of Argonaute proteins, suggesting that a form of the transient amplifying complex is conserved, but that GLH-1 is not limited to just piRNA amplification. This comparative approach represents a significant advance toward understanding how GLH-1/Vasa functions as a multipotency factor within and outside of the germline.

Materials and Methods

Strain generation and maintenance

C. elegans strains were maintained using standard protocols (Brenner 1974). See Supplemental Material, Figure S2 for a complete list of GLH-1::GFP::3xFLAG alleles. Additional strains created for this study include DUP121 *glh-1(sam24[glh-1::gfp::3xFLAG]) I*; *pgl-1(sam52[pgl-1::mTagRFPT::3xFLAG]) IV*, DUP162 *glh-1(sam24[glh-1::gfp::3xFLAG])I* ; *itIs37[pie-1p::mCherry::H2B::pie-1 3′UTR, unc-119(+)]IV*, DUP163 *glh-1(sam92[glh-1(DQAD)::gfp::3xFLAG]) I*; *itIs37[pie-1p::mCherry::H2B::pie-1 3′UTR, unc-119(+)] IV*, DUP165 *glh-2(sam82[glh-2(DQAD)]) glh-1(sam92[glh-1(DQAD)::gfp::3xFLAG]) I*; *itIs37[pie-1p::mCherry::H2B::pie-1 3′UTR, unc-119(+)] IV*, DUP178 *glh-1(sam24[glh-1::gfp::3xFLAG]) prg-1(sam97[mTagRFP::3xFLAG::PRG-1]) I*, DUP180 *glh-1(sam65[Δglh-1::gfp::3xFLAG]) prg-1(sam97[TagRFP::3xFLAG::PRG-1]) I*, DUP181 *glh-1(sam92[glh-1(DQAD)::gfp::3xFLAG]) prg-1(sam97[TagRFP::3xFLAG::PRG-1]) I*, and DUP184 *glh-1(sam86[glh-1(_EAD)::gfp::3xFLAG]) prg-1(sam97[TagRFP::3xFLAG::PRG-1]) I*. All strains generated for

this study and their associated sequence files are available upon request. Experimental sample sizes for the *C. elegans* experiments were done in excess for a 95% C.I. and a 5% margin of error relative to the expected population size (*i.e.*, the number of progeny on a worm plate).

Screen design

EMS mutagenesis was performed in DUP64 *glh-1(sam24[glh-1::GFP::3xFLAG]) I* worms using the standard protocol (Kutscher and Shaham 2014). Adult grandchildren (F2s) were then screened under a Leica M165FC fluorescence stereomicroscope (Leica Biosystems, Buffalo Grove, IL) for changes in P-granule appearance as visualized with the GLH-1::GFP::3xFLAG reporter. Sequencing of *glh-1* was performed for several mutants exhibiting aberrant GLH-1::GFP phenotypes.

CRISPR strain construction

Creation of the *glh-1(sam24[glh-1::GFP::3xFLAG]) I* allele was previously described (Andralojc *et al.* 2017). A co-CRISPR technique with *dpy-10* was used to create the mutant alleles as described (Paix *et al.* 2017). Table S1 lists the sequences for the guide RNA and repair templates for the strains created. An mTagRFPT::3xFLAG tag was added to the C-terminus of *pgl-1* and the N-terminus of *prg-1*, using the fluorescent protein-selection excision cassette (FP-SEC) method, to create *pgl-1(sam52)* and *prg-1(sam97)* alleles (Dickinson *et al.* 2015). The same method was modified to generate the *glh-1(sam31)* allele found in DUP73, which contains a bicistronic rSL2 GFP::3xFLAG transcriptional *glh-1* reporter. All edits generated for this study were sequence verified, and sequence and GenBank files for each strain are available upon request.

Fertility assay

For each strain, the fertility was determined by plating L4 worms at both 20° and 26°. Hatched F1 progeny were then picked to 10 plates with 25 worms on each plate. The percent of grotty (uterus filled with unfertilized oocytes and terminal embryos) and clean (germline atrophy with empty uterus) sterile F1s were scored when they reached day 2 of adulthood.

Embryonic lethality

For each strain, embryonic lethality was determined by plating L4 worms at 20°. Hatched F1s were grown to adulthood, and six worms were picked to new plates and allowed to lay for 5 hr. Embryos were marked and counted, and unhatched embryos were counted again 18–24-hr later. Terminal phenotypes were imaged from these unhatched, but still moving, embryos.

Imaging, P-granule counts, and expression intensity

Live worms were mounted on agarose pads in egg buffer (25 mM HEPES, 120 mM NaCl, 2 mM $MgCl_2$, 2 mM $CaCl_2$, 50 mM KCl, and 1 mM levamisole) and imaged with a 63× objective under fixed exposure conditions. A single plane focused midway through the germline loop region was acquired for 10 worms from each strain using Leica AF6000 acquisition software on an inverted Leica DMI6000B microscope with an attached Leica DFC365FX camera. ImageJ was used to count P granules and average GFP intensity within the field of view.

To measure P-granule size in P4 cells (Figure 5), live embryos from DUP162, DUP163, and DUP165 were mounted on agarose slides and focused midway through P4 nuclei using the mCherry::H2B signal. Both mCherry and GFP were acquired with fixed exposure conditions at this single focal plane. ImageJ was used to identify and calculate P-granule areas in ≥ 40 embryos from each strain.

For higher-resolution images, the same microscope and objective was used to acquire Z sections through 10 μm, and then images were deconvolved and shown as a maximum intensity projection. All scale bars represent 20 μm. For immunostained images (Figure 4 and Figure 7), worms and embryos were fixed and stained with anti-GFP monoclonal and anti-PGL-1, or anti RPL-7a [E109, Cell Signaling Technologies, Inc. (CST), Danvers, MA], polyclonal antibodies as previously described (Andralojc *et al.* 2017).

Next, 18S rRNA FISH was performed using Biosearch Technologies Stellaris smFISH probes, a set of 48 tandem probes targeting *rrn-1.1*, and conjugated with CAL Fluor red 590. Hybridization was performed as described previously (Ji and van Oudenaarden 2012; Campbell and Updike 2015).

Liquid culture

For each of the DUP64, DUP73, DUP171, and DUP 173 strains, 25 plates were grown until gravid and then bleach-treated to harvest embryos. Hatched embryos were used to seed 250 μl of S Media (separated into four 1-liter flasks) containing freeze-dried OP50 (LabTie, Leiden, The Netherlands) on the following day. Worms were grown in liquid culture and until most reached the young adult stage with embryos in the uterus, and were then harvested, washed, and bleach-treated to synchronize development. L1-stage worms hatched without food were then used to inoculate another 250 μl of S Media with OP50. Worms were grown until the majority reached the young adult stage, where they were harvested, washed, and flash frozen in 1-ml aliquots.

Preparation of protein lysate

First, 1–2 ml of frozen worms grown from liquid culture were removed from the −80, ground with a mortar and pestle in liquid nitrogen for 15 min, and then resuspended in 7 ml of cold lysis buffer [25 mM HEPES-KOH (pH 7.4), 10 mM KOAc, 2 mM $Mg(OAc)^2$, 100 mM KCl, 0.25% Triton X-100, 1 mM PMSF, one proteinase inhibitor tablet, 1:200 Riboguard, and 1:200 DNase]. Samples were then spun at 5000 rpm for 5 min and supernatants were then immediately used for IP.

IP analysis

Anti-DYKDDDDK agarose beads (Fujifilm Wako Chemicals, Richmond, VA) were removed from the −20, allowed to equilibrate for 10 min, and were then inverted to resuspend the beads. Next, 100 μl of the bead suspension was aliquoted into seven Eppendorf tubes and 1 ml of cold 1× TBS was added to each tube. Beads were then spun at 4° for 1 min at 1200 rpm. Supernatant was removed and beads were washed with 1 ml of cold 1× TBS and then centrifuged at 4° for 1 min at 1200 rpm. The supernatant was removed with a pipette and then the TBS wash was repeated two more times. After the last wash, 1 ml of the protein lysate was pipetted into each of the seven Eppendorf tubes with agarose beads. Tubes were inverted for mixing and then placed on a rotator at 4° for 3 hr. After 3 hr, all the tubes were spun at 4° for 1 min at 1200 rpm. The supernatant, which contained the unbound fraction, was removed, and then beads were washed and spun three times with 1 ml of 1× TBS. During the third wash, 10 μl was removed and imaged to confirm that the GFP-tagged protein was attached to the beads (see imaging agarose beads section). Beads from all seven tubes were combined into one Eppendorf tube and flash frozen in liquid nitrogen. Beads with protein still bound were then sent to cell signaling technologies (CST) for MS.

Next, 15 μl of anti-DYKDDDDK agarose beads under control or protein-exposed conditions were imaged under DIC and GFP with a 10× objective on a Leica DMI6000B microscope (Figure S3). A western blot was used to demonstrate that conditions were optimal for GLH-1::GFP::3xFLAG IP.

MS and analysis

The MS analysis was performed by CST (using their PTMScan Discovery service). On-bead protease digestion was performed followed by C18 solid-phase extraction, peptide lyophilization, and antibody enrichment of post-translational modification-containing peptides using CST-developed antibodies. Then, peptides were loaded onto a 50 cm × 100 μm PicoFrit capillary column packed with C18 reversed-phase resin for LC-MS/MS. The MS parameters were as follows: MS run time 168 min, MS1 scan range (300.0–1500.00), and top 20 MS/MS (minimum signal 500, isolation width 2.0, normalized collision energy 35.0, activation-Q 0.250, activation time 20.0, lock mass 371.101237, charge state rejection enabled, charge state 1 + rejected, dynamic exclusion enabled, repeat count 1, repeat duration 35.0, exclusion list size 500, exclusion duration 40.0, exclusion mass width relative to mass, and exclusion mass width 10 ppm). MS informatics were also done by CST. The MS/MS spectra were evaluated using SEQUEST (Eng *et al.* 1994) and the core platform from Harvard University. Searches were performed against the most recent update of the WormBase *C. elegans* database, with mass accuracy of ±50 ppm for precursor ions and 0.02 kDa for product ions. Results were then filtered with mass accuracy of ±5 ppm on precursor ions and presence of the intended motif. These were then further filtered to a 1% protein false discovery rate. Analysis results are included in Table S2, which has also been uploaded to the PRIDE (PRoteomics IDEntifications) proteomics repository, project accession PXD014135.

Data availability

All strains generated for this study and their associated sequence files are available upon request. Analysis results are included in Table S2, which has also been uploaded to the PRIDE proteomics repository, project accession PXD014135. Supplemental material available at FigShare: https://doi.org/10.25386/genetics.9497666.

Results

GLH-1 is just one of several dozen proteins enriched in germ granules—also known as P granules—in *C. elegans*, but like Vasa, it is part of a germ granule protein core that is conserved across multicellular animals. GLH-1 is a constitutive P-granule protein, meaning that it associates with P granules at all stages of adult and embryonic development (Figure 1A). Other core germ granule proteins include those carrying Tudor domains and Argonaute proteins that bind small RNAs (Figure 1B). The function of this protein core in germ granules is both intriguing and elusive, but studies across systems have demonstrated a role for this core in regulating protein expression and small RNA biogenesis in ways that ensure germ cell integrity. GLH-1 has three close paralogs (GLH-2, GLH-3, and GLH-4), but only GLH-1 and GLH-2 contain all the domains that define Vasa proteins. Vasa-defining domains include a glycine-rich repeat domain, a flanking domain that wraps in between N- and C-terminal DEAD-box helicase domains, and a negatively charged domain that precedes a terminal tryptophan (Figure 1C and Figure S1, A and B). A conserved zinc-knuckle domain can be found in most Vasa homologs, but has been lost several times throughout evolution (Gustafson and Wessel 2010) (Figure S1C). GLH-1 mutations, including nulls, are fertile at the permissive temperature of 20° but are sterile at 26° (Kuznicki *et al.* 2000). This temperature-sensitive (ts)-sterile phenotype stems from redundancy with other GLHs, as both *glh-2 glh-1* and *glh-1*; *glh-4* double mutants are sterile at permissive temperatures, and exhibit a severe reduction or no germ cells, and little to no sperm [Spike *et al.* (2008) and this study]. The *C. elegans* genome encodes ∼50 DEAD-box helicases. Of these, the GLHs, RDE-12, VBH-1, LAF-1, DDX-19, and DDX-17 have glycine-rich repeats and (with the exception of DDX-17) have previously been shown to associate with P granules (Gruidl *et al.* 1996; Hubert and Anderson 2009; Sheth *et al.* 2010; Shirayama *et al.* 2014); however, outside GLH-1 and GLH-2, none contain a full repertoire of Vasa domains (Figure 1C).

The structure of *Drosophila*'s Vasa-flanking and helicase domains have been determined, showing that the N- (blue) and C-terminal (green) RecA-like DEAD-box domains interact upon RNA and ATP binding (Figure 1D, Sengoku *et al.* 2006). ATP hydrolysis is coupled with RNA helicase activity,

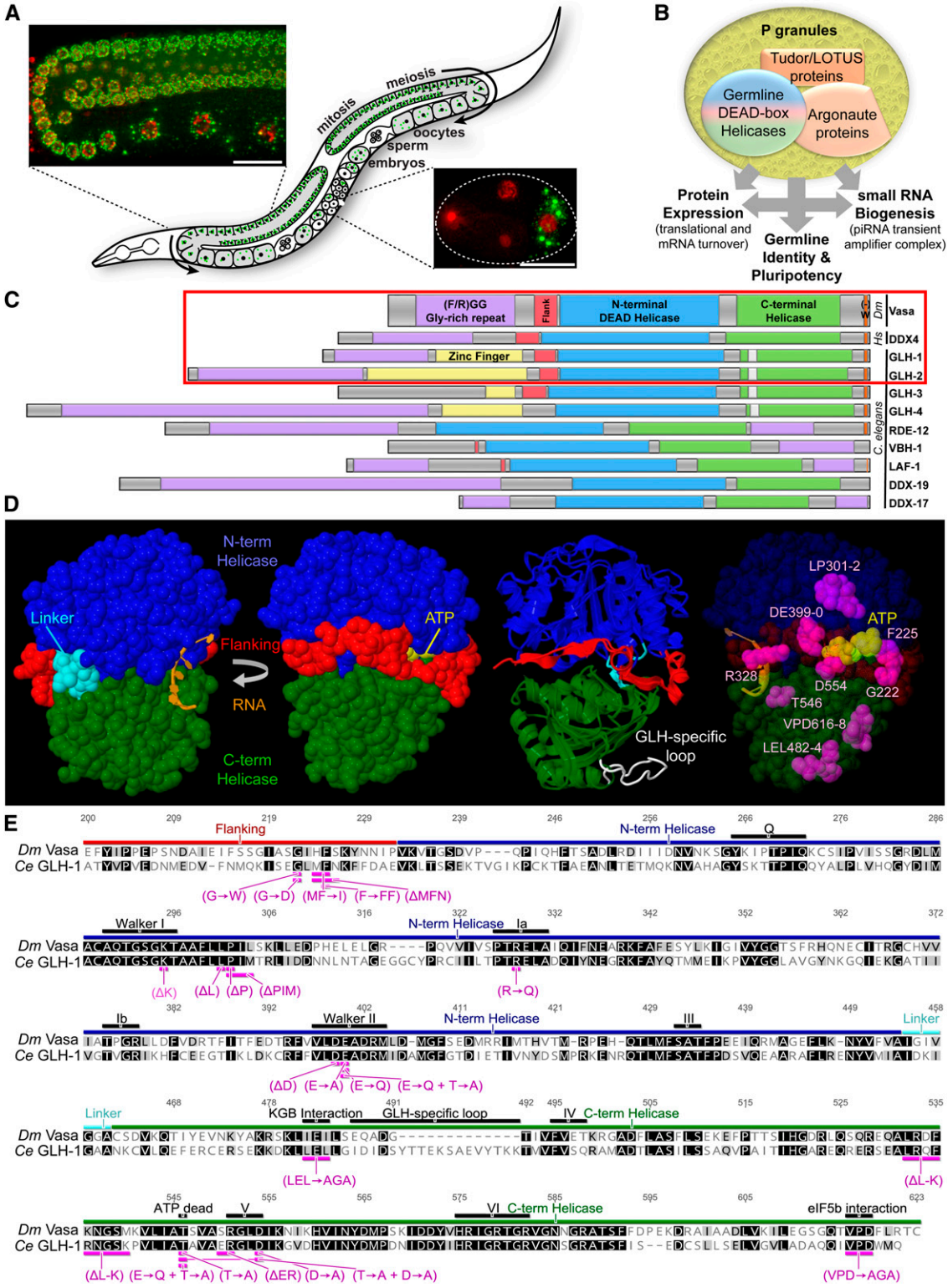

Figure 1 GLH Proteins in the *C. elegans* germline. (A) GLH-1::GFP::3xFLAG in P granules and mCherry:His2B-marked chromatin. Inserts provide context for expression in the germline loop and four-cell embryo. (B) Schematic depicting the function of core proteins in P granules. (C) Conservation of Vasa/DDX4-like DEAD-box helicases in *C. elegans*. A red box surrounds proteins that contain all four Vasa-defining domains (glycine-rich in purple, flanking in red, N- and C- terminal helicase in blue and green, and negatively charged residues before a terminal tryptophan in orange). The GLH-specific loop is shown in white. (D) Crystal structure of Vasa showing front and back views of the flanking and helicase domains, in relation to ATP- and RNA-binding pockets [as determined by Sengoku *et al.* (2006)]. Image 3 is an overlay of Vasa (ribbon) with an iTasser-predicted model of GLH-1 (backbone) that shows the location of the GLH-specific loop (white). Image 4 shows key amino acid residues targeted in this study and their location within the Vasa protein structure. (E) Sequence alignment of the flanking and helicase domains in *Drosophila* Vasa with *C. elegans* GLH-1. Protein domains and mutations are indicated (purple). The K295A mutation was not obtained. The ΔER550-1 was not sustainable. See also Figure S1. *Ce*, *C. elegans*; ; *Dm*, *Drosophila melanogaster*; *Hs*, *Homo sapiens*; piRNA, piwi-interacting RNA.

destabilizing RNA duplexes in a nonprocessive manner. The flanking domain (red) wraps around the side when the helicase domains are in the closed conformation. Because of the high conservation between Vasa in *Drosophila* and GLH-1 in *C. elegans* (Figure 1E), iTasser was used to model the structure of GLH-1 based on Vasa (Figure 1D, third image overlay). Except for a GLH-specific loop (white), the predicted structure was nearly identical. From this, several key residues, and their relation to ATP- and RNA-binding sites and helicase interphases, can be identified (Figure 1D, fourth image).

New alleles of *glh-1* were initially obtained from an EMS mutagenesis screen for P-granule phenotypes. Unlike previous screens that utilized transgenes expressed from an array, this screen was performed in a strain where endogenous GLH-1 was tagged with GFP::3xFLAG, allowing for the recovery of intragenic mutations. While most *glh-1* alleles from the screen attenuated GFP expression, one allele dispersed GLH-1::GFP throughout the cytoplasm and resembled GLH-1 staining patterns previously associated with original *glh-1* alleles (Spike *et al.* 2008). Sequencing *glh-1* revealed a Gly to Asp (G→D) change (Vasa position 222) caused by a single-base pair mutation within the flanking domain, suggesting that flanking domain function is required for GLH-1's association with P granules (Figure 2A). Until now, the function of Vasa's flanking domain was unknown because alleles within this domain did not previously exist. CRISPR was used to generate four additional alleles with mutations in the flanking domain, and all recapitulated the GLH-1::GFP dispersal phenotype (Figure S2 and Table S1). GLH-1-granule dispersal and expression intensity was quantified in 10 gonad arms under fixed exposure conditions, as was the impact on embryonic lethality and fertility at permissive and restrictive temperatures (Figure 3 and Figure S2). At both permissive and restrictive temperatures, the parental GLH-1::GFP::3xFLAG fusion is fully wild-type, with perinuclear GLH-1 granules and no defects in fertility. For comparison, a complete *glh-1* deletion (Δ*glh-1*) that expresses only GFP::3xFLAG and a *glh-1* transcriptional reporter (GFP::3xFLAG separated from *glh-1* with an intercistronic rSL2 spacer, *glh-1* Txn GFP, Figure 2A) were generated from the parental strain. Interestingly, GFP expression in the deletion is almost three times as bright, suggesting that GLH-1 protein negatively autoregulates its own expression. Fertility defects at the restrictive temperature for flanking-domain mutations are comparable to the *glh-1* deletion, showing that these flanking-domain mutations reflect the phenotype of null alleles.

To see if compromising GLH-1 helicase activity also caused its dispersal, 12 additional strains were created that either replicated canonical *Drosophila* alleles of Vasa in endogenous GLH-1::GFP::3xFLAG or introduced changes in key conserved residues (Figure 1E) (Sengoku *et al.* 2006; Dehghani and Lasko 2015, 2016). Attempts to generate a K→A mutation in the Walker I motif (Vasa position 295) to knock out helicase activity were unsuccessful, but yielded three mutations (ΔL, ΔP, and ΔPIM) immediately to the right of the Walker I motif that all had the dispersed GLH-1::GFP phenotype (Figure 3 and Figure S2). Subsequently, a T→A mutation was generated just before motif V (Vasa position 546) that had previously been shown to abolish the ATPase activity of Vasa *in vitro* (Sengoku *et al.* 2006), and this allele dispersed GLH-1 and caused fertility defects at the restrictive temperature (Figure 2A and Figure 3). The DEAD-box in motif II is also essential for ATP hydrolysis (Pause and Sonenberg 1992), so a deletion of the aspartic acid (D) residue from the DEAD-box (_EAD) was generated (Vasa position 399), as was an E to A (D**A**AD) substitution (Vasa position 400), both of which dispersed GLH-1 with ts-fertility defects (Figure 2A and Figure 3). When the _EAD deletion and the D**A**AD substitution were put into both *glh-1* and *glh-2* to create double mutants, they resulted in fertility defects at both permissive and restrictive temperatures (Figure 3). At least some of these 17 mutations in the flanking and helicase domains affected the activities of adjacent domains, but since most were point mutations, it would be unlikely for them all to have a structural impact. So when taken together, these results suggest that (1) helicase activity is required for fertility, (2) GLH-1 associates with germ granules by virtue of its helicase activity and not through its structural motifs, (3) that the flanking domain is integral to the helicase activity, and that (4) helicase activity is not required for GLH-1 to negatively autoregulate its expression.

Vasa was identified as a component of a transient Amplifier complex that mediates piRNA amplification in what is called the ping-pong loop (Xiol *et al.* 2014; Wenda *et al.* 2017). This association between Vasa and Argonaute proteins that mediates ping-pong amplification was detected using a Vasa D**Q**AD mutation (position 400), which is thought to prevent the release of ATP hydrolysis products, facilitating the accumulation of larger Vasa-containing aggregates. While *C. elegans* use a ping-pong-independent method to amplify piRNA-mediated silencing, we sought to determine whether Argonaute proteins could be detected when D**Q**AD substitutions were introduced into GLH-1, or both GLH-1 and GLH-2 (Figure 2A). Unlike _EAD and D**A**AD, the D**Q**AD substitution is more severe than the *glh-1* deletion, meaning that worms are less fertile at 20° and most of the embryos arrest during elongation (Figure 2B and Figure 3). Also, instead of being completely dispersed in the cytoplasm like _EAD and D**A**AD, D**Q**AD causes some GLH-1 to accumulate in large cytoplasmic aggregates, primarily in the shared cytoplasm of the distal germline (Figure 2C). Embryonic lethality and large aggregate formation of GLH-1(D**Q**AD) becomes more pronounced when the D**Q**AD substitution is also introduced into GLH-2. In the double GLH-1(DQAD) GLH-2(DQAD) mutant, large GLH-1::GFP(D**Q**AD) aggregates are no longer cleared from somatic blastomeres, and some persist in various somatic cells during larval development (Figure 2C). These double mutants can be passaged for only a couple of generations and must be maintained over a balancer. It should be noted that while these large aggregates have been ascribed as a specific

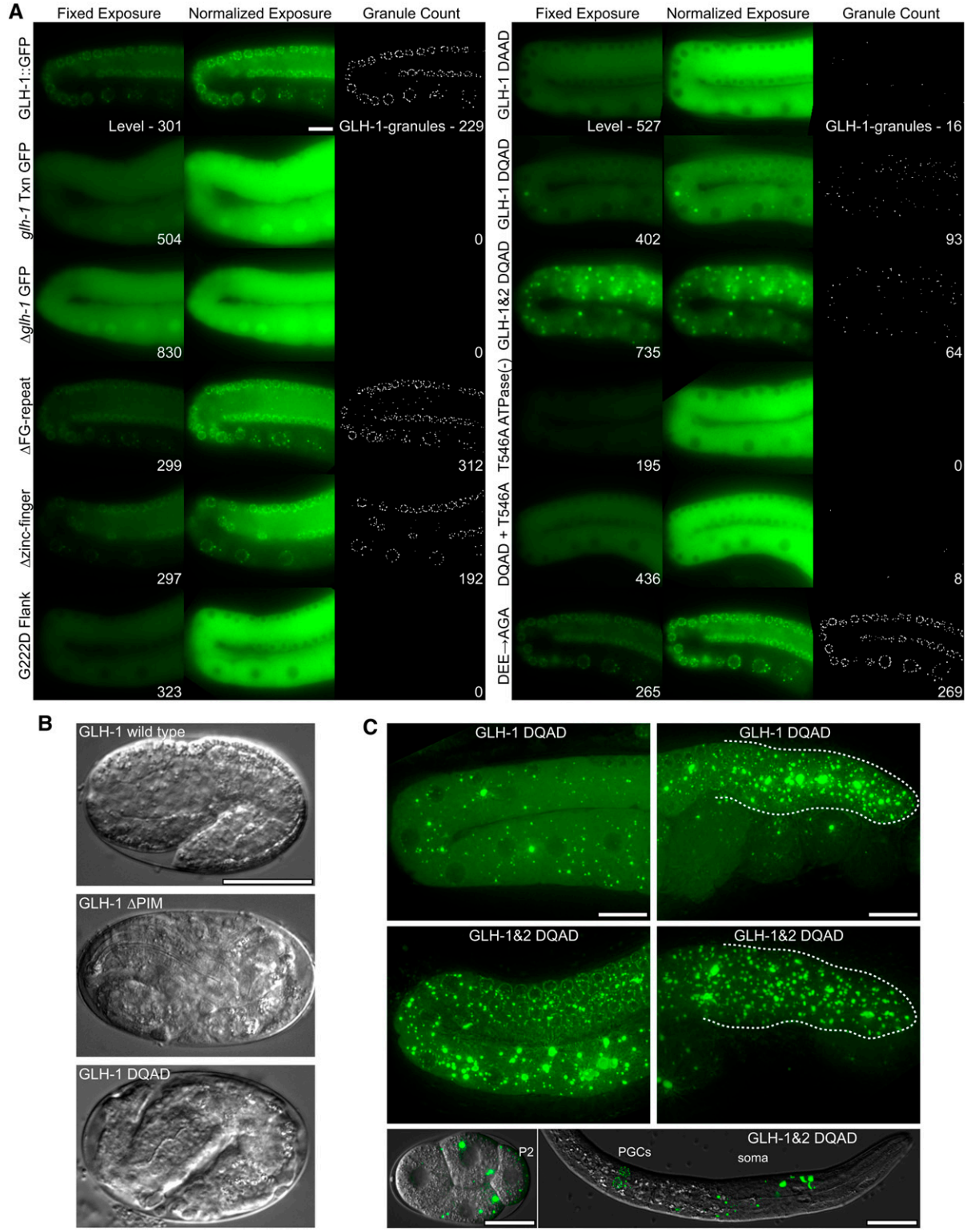

Figure 2 Level and distribution of mutant forms of GLH-1 in *C. elegans*. (A) GLH-1::GFP::3xFLAG expression in the germline loop. Fixed exposures (left) were normalized (middle) to better view the distribution of fluorescence. GLH-1 granules were quantified using ImageJ (right). In ΔPIM and DQAD mutants, embryos arrest in the elongation phase. (C) GLH-1(DQAD)::GFP::3xFLAG accumulation in proximal (left) and distal (right) germlines is enhanced in GLH-2(DQAD). In double mutants, GLH-1(DQAD) aggregates persist in somatic blastomeres and the soma of hatched worms (bottom). Quantification was performed on images from 10 worms for each strain (see Figure S2). PGC, primordial germ cell.

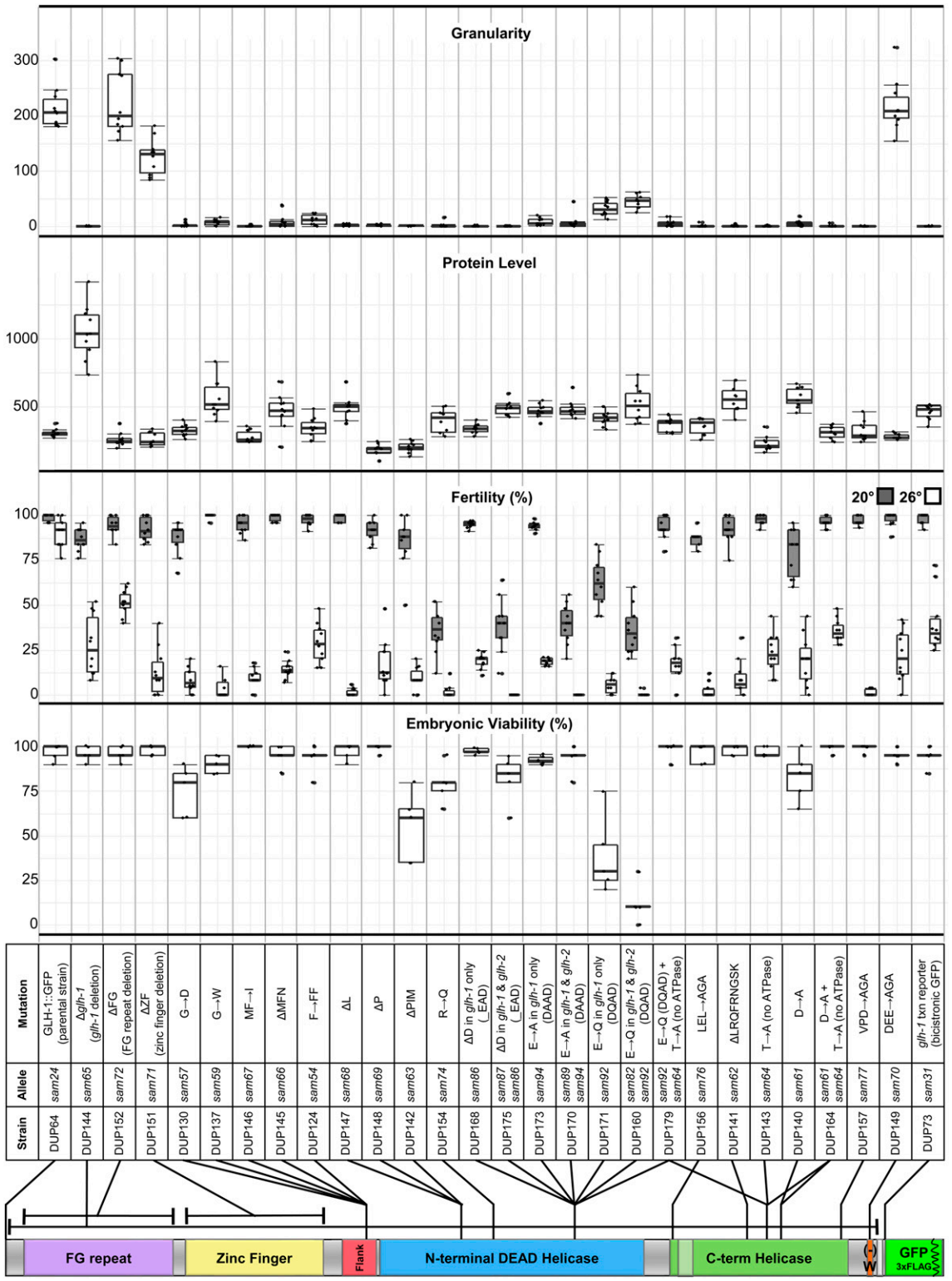

Figure 3 Consequences of GLH-1 mutant alleles. From top to bottom: comparison of granularity (GLH-1 granules), GLH-1 protein level, fertility at permissive (20°) and restrictive (26°) temperatures, and embryonic viability in GLH-1 mutants. Mutation details, strains, and allele names and their respective locations are indicated. Replicates for each of the four assays are provided in the *Materials and Methods*. Box plots represent quartiles above and below the median with whiskers extending 1 SD from the mean. See also Figure S2. C-term, C-terminal.

transient state, their observation in D**Q**AD, but not in _EAD or D**A**AD, introduces the possibility that D**Q**AD creates a neomorphic allele prone to unspecific germline aggregate formation. The impact of the D**Q**AD mutant has not been thoroughly characterized *in vivo*, and existing data from *in vitro* experiments are not enough to understand why

_EAD and D**A**AD disperses GLH-1 or Vasa, while D**Q**AD causes them to aggregate. A prevailing and speculative assumption is that mutations like _EAD and D**A**AD inhibit the binding of ATP and RNA substrates, while in D**Q**AD these substrates are bound but not released. Further biochemical characterization of these mutations will be needed to confirm whether this is the case.

GLH-1 has been positioned upstream of PGL proteins in the embryonic P-granule assembly pathway, but in adult germlines the association is more mutualistic (Kuznicki *et al.* 2000; Kawasaki *et al.* 2004; Hanazawa *et al.* 2011; Updike *et al.* 2011). Both PGL-1 and GLH-1 colocalize at all stages of development in wild-type animals, except for a brief resurgence of small somatic PGL-1 granules around the 30–50-cell stage of embryogenesis (Figure 4A). Even though PGL-1 is dispersed in early GLH-1(G222D) mutant embryos, it reassembles into P granules despite the dispersal of GLH-1(G222D) at the four-cell stage, and largely stays associated with P granules in the adult germline (Figure 4B). A similar pattern is observed with mCherry-tagged PRG-1, the PIWI Argonaute in *C. elegans*, which maintains its association with P granules in the adult germline in Δ*glh-1* and GLH-1(_EAD) mutants (Figure 4D). In contrast, large GLH-1(D**Q**AD) aggregates contain both PGL-1 and PRG-1 (Figure 4, C and D). Taken together, these results suggest that most It is possible that the proteins are largely unaffected when GLH-1 is deleted or dispersed. In contrast, large GLH-1(D**Q**AD) aggregates sequester or retain P-granule proteins, and potentially impair their normal function.

It is possible that the GLH-1(D**A**AD) mutation inhibits ATP binding or hydrolysis, maintaining the N- and C-terminal domains in their open configuration, while the D**Q**AD mutation remains bound to hydrolyzed ATP with N- and C-terminal domains closed, as has been proposed for Vasa. In that case, an indirect assessment would be to inhibit ATP hydrolysis to see if it suppresses the embryonic lethality and fertility defects of D**Q**AD. To assess this possibility, CRISPR was used to generate the (D**Q**AD) + (T to A) (Vasa position 546) double mutant. This strain no longer exhibited large GLH-1 aggregates (Figure 2A), and the fertility defects and embryonic lethality were suppressed at the permissive temperature (Figure 3). These results support work in other systems that suggest D**Q**AD aggregates are locked in a closed-conformation transient state (Xiol *et al.* 2014; Dehghani and Lasko 2016; Wenda *et al.* 2017).

One Vasa mutation shown to uncouple ATP hydrolysis from its helicase activity *in vitro* is D to A (Vasa position 554), which lies at the interphase of Vasa's N- and C-terminal helicase domains (Sengoku *et al.* 2006). This mutation also has a mild dominant negative phenotype in *C. elegans*, showing increased embryonic lethality and fertility defects (Figure 3). To determine if this could be caused by GLH-1 expending ATP but not coupling it with helicase activity, the analogous T546A was introduced to inhibit ATPase activity (Figure S2). This double mutant suppressed both the embryonic and fertility defects of the D554A mutant (Figure 3). To further test this idea, an R to Q mutation (Vasa position 328) was engineered to disrupt helicase activity in the RNA-binding pocket with minimal impact on helicase structure, potentially uncoupling helicase activity from ATP hydrolysis. Like D554A, R328Q alleles also enhanced embryonic lethality and fertility defects (Figure 3). These alleles may suggest that expenditure of ATP uncoupled from helicase activity drives dominant Vasa and GLH-1 phenotypes. Two additional C-terminal helicase alleles were created to disrupt previously reported binding sites for KGB-1 (LEL→AGA) and eIF5b (VPD→AGA); however, both dispersed GLH-1 and looked like other helicase mutations (Figure 3).

Outside of the flanking and helicase domains there are three Vasa-specific motifs: a glycine-rich FG repeat, a zinc-knuckle/finger, and a terminal tryptophan immediately preceded by three negatively charged amino acids. Unlike mutations in the flanking and helicase domains, deletions and substitutions in these motifs have no or very little effect on GLH-1's association with P granules in the adult germline (Figure 2A); however, each show compromised fertility at the restrictive temperature (Figure 3). While this demonstrates that GLH-1 function can still be impaired despite showing proper P-granule localization, it came as a surprise for the ΔFG-repeat strain since FG repeats were previously shown to facilitate contact with the nuclear periphery when ectopically expressed (Updike *et al.* 2011). Vasa proteins contain these glycine-rich repeats, which are interspersed with either arginines or phenylalanines [reviewed in Marnik and Updike (2019)]. These are intrinsically disordered motifs, and in the case of the FG repeats of GLH, the interspersed phenylalanines form hydrophobic tethers with FG repeats in the nuclear pore complex (NPC) to maintain a wetting-like appearance on the nuclear periphery (Figure 5). Unlike the adult germline, deletion of the FG repeat in embryos caused larger GLH-1::GFP granules in primordial germ cells and their precursors, and deleting the FG repeat of GLH-2 in this background further increased GLH-1::GFP granule size (Figure 5, A and B). Moreover, GLH-1 granules in these double mutants appeared more spherical, suggesting that they had lost contacts that adhered them to the nuclear periphery. One potential role for FG-repeat tethering is to maximize coverage of NPCs so that nascent transcripts are captured by P granules as they exit the nucleus. Another might be to ensure the symmetric distribution of P granules as the P4 precursor divides into the two primordial germ cells, but no evidence supporting this was observed in the double mutant. It is also possible that the FG repeats found in GLH-4, RDE-12, and DDX-19 function redundantly to mask an asymmetric distribution phenotype when FG repeats are deleted from GLH-1 and GLH-2.

To get an idea of which proteins are loosely associated with GLH-1, and how these associations change when enzymatic activity is compromised in D**Q**AD and D**A**AD mutants, GLH-1::GFP::3xFLAG was immunoprecipitated with anti-FLAG agarose beads and replicates were submitted for LC-MS/MS analysis (Figure 6 and Figure S3). Pairwise comparisons

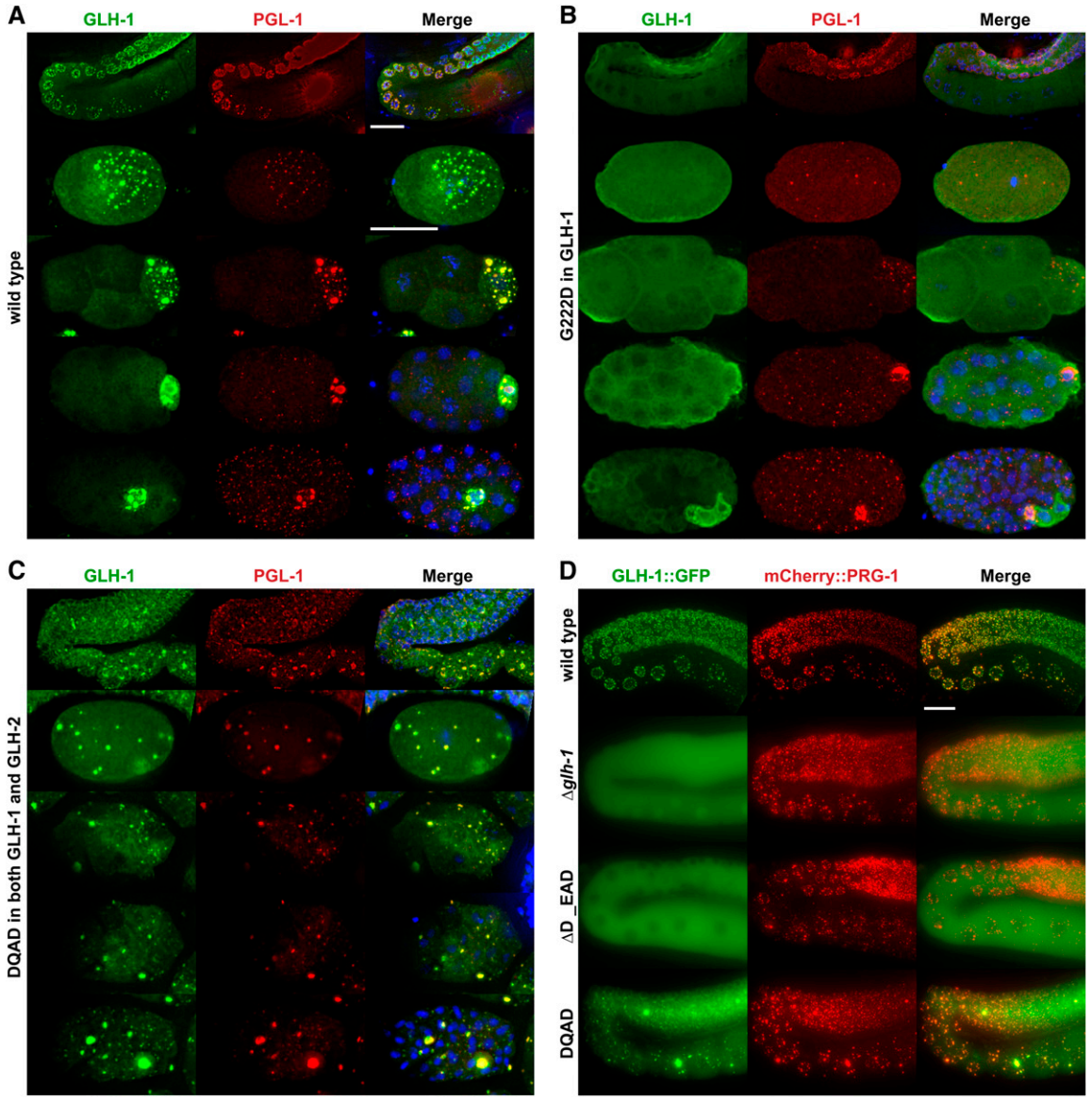

Figure 4 Colocalization of P-granule components in wild-type and GLH-1 mutants. (A–C) Immunostaining of GLH-1 (green) and PGL-1 (red) in fixed germlines, and 1-, 4-, 16-, and 32-cell embryos. (D) GLH-1::GFP and mCherry::PRG-1 in the germline of living worms. At least 10 worms were imaged for each indicated genotype.

between the *glh-1* transcriptional reporter driving GFP::3xFLAG alone identified GLH-1-enriched proteins (Figure S2). As a proof of principle, NPC proteins and transport factors were identified among the 2505 proteins from the LC-MS/MS analysis (Figure 6, left column, blue and Figure S3). NPCs facilitate the interaction of P granules at the nuclear periphery and, when targeted by RNA interference (RNAi), several of them cause P granules to detach and distribute in the cytoplasm (Updike and Strome 2009; Voronina and Seydoux 2010). On average, NPCs are enriched in the GLH-1 IP, and this enrichment shows a significant decrease (left shift, DEAD to DAAD *P*-value = 0.0001 and DEAD to DQAD *P*-value = 0.0012) in both the DAAD and DQAD mutants, as would be expected with the dispersal of GLH-1 from the nuclear periphery in the mutants, confirming the robustness of the GLH-1 IP (Figure 6).

Gene ontology was examined in the enriched subsets ($>$ 2.5-fold normalized increase, *P*-value $<$ 0.05, Table S2), which identified most subunits of three evolutionarily conserved, multilobed scaffolding complexes collectively known as PCI complexes or zomes (Li *et al.* 2017). These include the COP9 signalosome, the regulatory Lid complex of the 26S proteasome, and the eIF3 translational initiation complex (Figure 6, left column, red; Table S3). One subunit of the COP9 signalosome called CSN-5 was previously identified through a yeast two-hybrid screen with GLH-1 as bait, and the interaction was confirmed through pull downs (Smith *et al.* 2002). Vasa-GST pull downs later confirmed that the

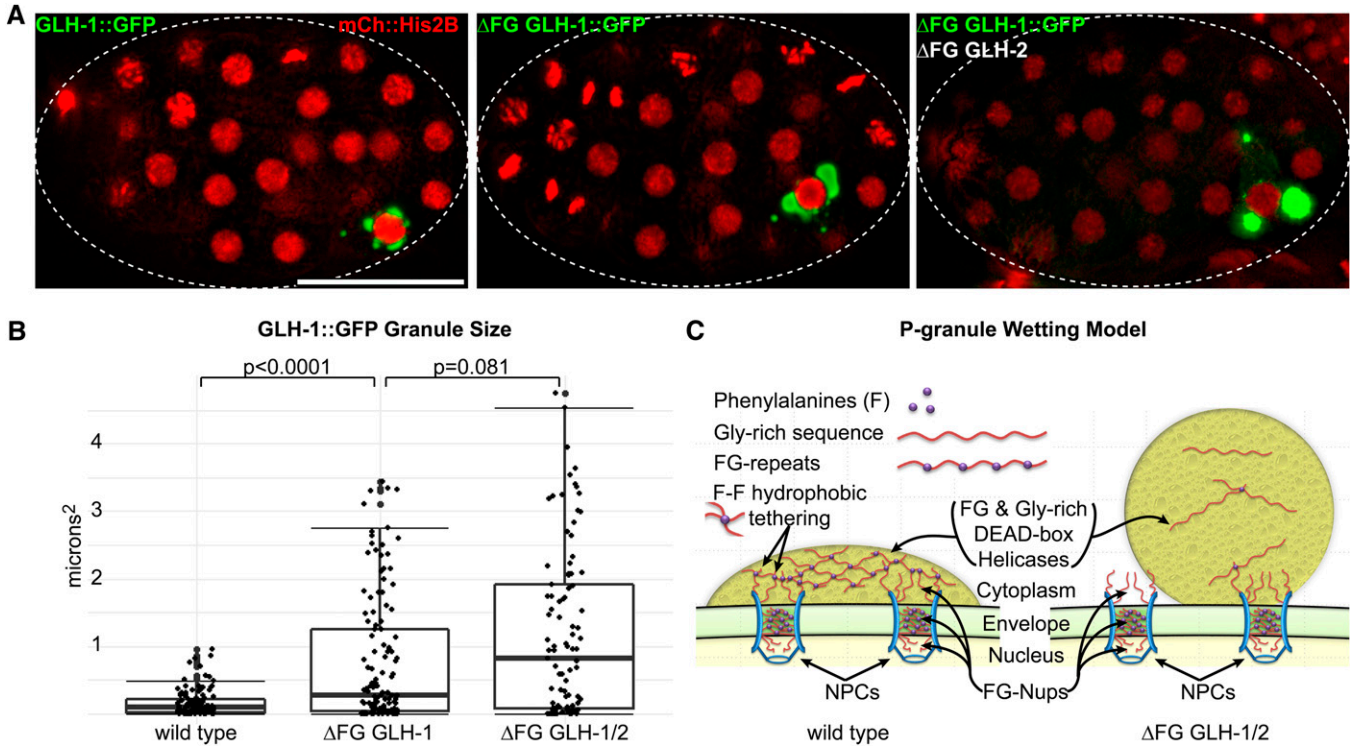

Figure 5 Glycine-rich FG repeats tether GLH-1 to the nuclear periphery. (A) Distribution of GLH-1::GFP (green) in the germline blastomere P4 of a wild-type embryo (left), an embryo lacking FG repeats in GLH-1 (middle), and an embryo lacking FG repeats in both GLH-1 and GLH-2 (right). mCherry::H2B (red) marks chromatin. (B) GLH-1-granule sizes in the germline blastomere P4 quantified using ImageJ. (C) Model depicting the hydrophobic tethering of P-granule FG-repeat domains to FG-nucleoporins (Nups) at the nuclear periphery. For size assays, P granules were counted from ≥ 40 embryos for each strain. Box plots show median quartiles and 1 SD above the mean. NPC, nuclear pore complex.

direct interaction with CSN5 is protective and evolutionarily conserved (Orsborn *et al.* 2007). This LC-MS/MS analysis supports these previous observations with CSN5, and further suggests that it is the structural conservation of all three PCI complexes that facilitates the interaction with GLH-1. As these interactions are compromised in D**A**AD and D**Q**AD mutants, they must be dependent upon GLH-1's enzymatic activity or P granule association.

Both the COP9 and Lid complexes modulate protein degradation by the 26S proteasome through deneddylation and deubiquitination, respectively [reviewed in Meister *et al.* (2016)]. Interestingly, subunits of the 20S core of the 26S proteasome were depleted in the GLH-1 IP, and this depletion is dampened (right shift) as GLH-1 became dispersed in the cytoplasm of D**A**AD and D**Q**AD mutants (Figure 6, middle column, blue). Whether GLH-1 is (1) sequestering these regulatory PCI complexes in P granules and away from the 20S proteasome core to antagonize protein degradation, (2) associating with the COP9 and Lid complexes prior to degradation in somatic blastomeres, or (3) facilitating the cycling of cullin-RING E3 ubiquitin ligase (CRL) activity still needs to be determined. Degradation of P granules in somatic blastomeres is mediated by CRL activity with the CCCH-finger-binding protein ZIF-1 acting as a receptor (DeRenzo *et al.* 2003; Oldenbroek *et al.* 2012). RNAi depletion of transcripts encoding multiple 20S core proteasome subunits, regulatory Lid subunits, and ubiquitins cause P-granule accumulation throughout the soma of arrested embryos (Updike and Strome 2009). Interestingly, *Drosophila* Vasa is also regulated through CRL activity by two CRL specificity receptors (Gus and Fsn) that compete for a single binding site on Vasa; the Gus receptor acts to stabilize Vasa and protect it from Fsn-mediated destabilization (Kugler *et al.* 2010). Gus and Fsn homologs were not enriched in our GLH-1 IP LC-MS/MS analysis, and the Gus-binding sites of Vasa do not appear conserved in GLHs; instead, in its place are ancestral CCHC zinc-knuckle motifs that have been independently lost in insects, tardigrades, vertebrates, and some sponges and flatworms (Figure S1C). While little is known about this motif in GLH-1, some evidence suggests that zinc knuckles may facilitate an interaction with an F-box containing a P-granule protein called PAN-1 (Gao *et al.* 2012). An intriguing possibility is that insects developed a convergent method using Gus and Fsn to protect Vasa from proteasome degradation, and that COP9 and Lid regulatory subunit sequestration by GLH-1 has a similar protective effect.

P granules may also act to exclude 40s and 60s ribosomes, whose proteins, like those of the 20S proteasome core, are depleted in the GLH-1 IP (Figure 6, middle column, red, Table S3). Again, this depletion is dampened (right shift) as GLH-1 becomes dispersed in the cytoplasm of D**A**AD and D**Q**AD mutants, suggesting that there is nothing inherent to the

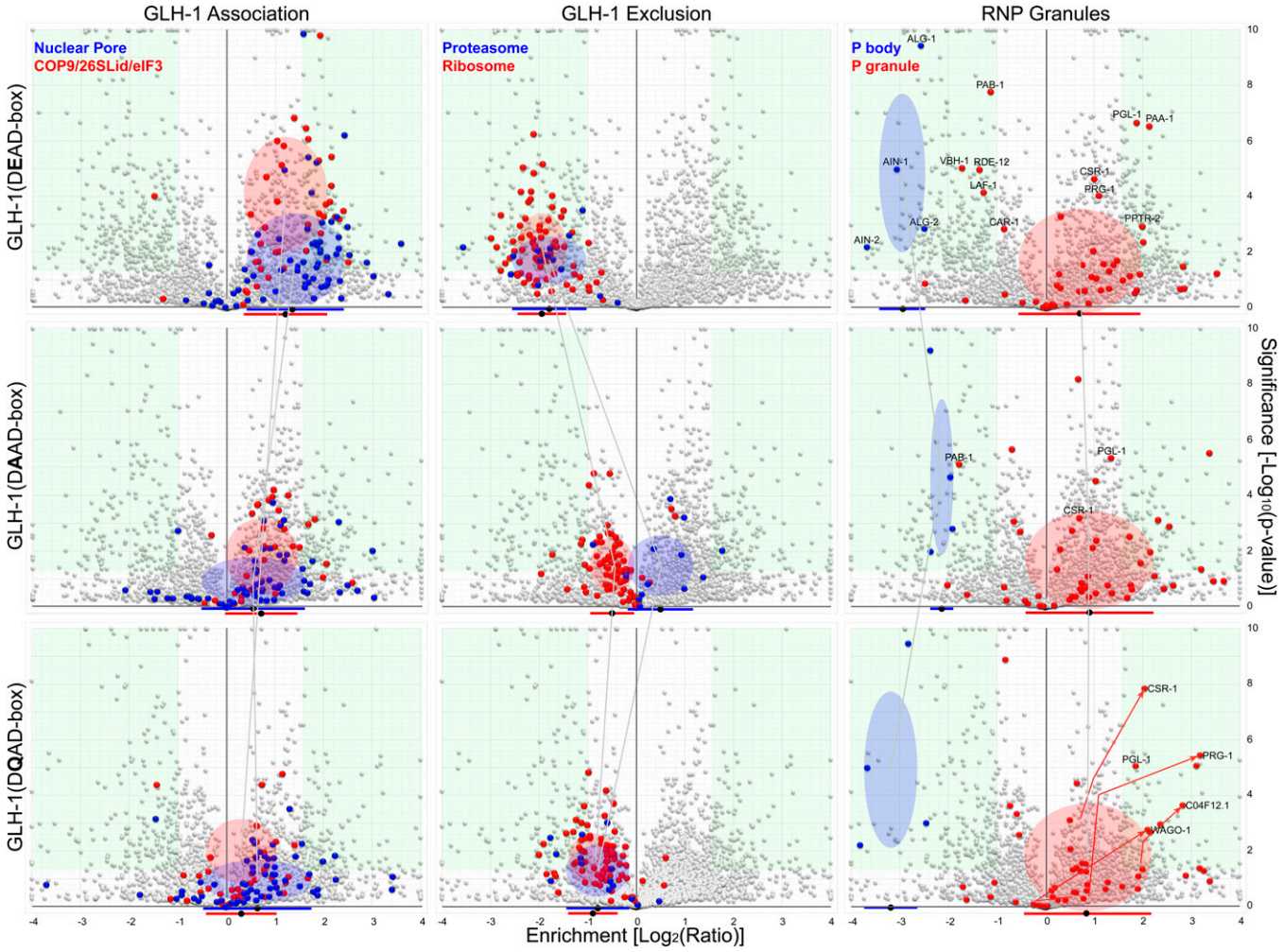

Figure 6 GLH-1 protein associations. Volcano plots show the significance and enrichment of proteins that immunoprecipitate with GLH-1::GFP::3xFLAG over the *glh-1* transcriptional reporter expressing GFP::3xFLAG alone, as identified by LC-MS/MS. Left column: protein families showing an enriched GLH-1 association include nuclear pore proteins (blue) and subunits of PCI scaffolding complexes. These associations decrease in DAAD (middle row) and DQAD (bottom row) mutants. Red and blue bars under the *x*-axis indicate the median and 1 SD, and colored ovals do the same but also indicate the distribution of significance. Green boxes show normalized enrichment and exclusion > 2.5-fold, and a *P*-value < 0.05. Nuclear pore genes used in this analysis are indicated in Table S3. Middle column: protein families showing stronger enrichment for GFP::3xFLAG alone include 20S core subunits of the 26S proteasome (blue) and subunits of the ribosome (red). Right column: proteins associated with RNP granules. P-body proteins (blue) and P-granule proteins (red). Data were obtained from two technical replicates for each indicated genotype. See also Table S3. LC, liquid chromatography; MS, mass spectrometry; PCI, 26S Proteasome Lid, COP9 Signalosome, and eIF3; RNP, ribonucleoproteins.

GLH-1 protein that repels ribosomes, but that the bulk of the GLH-1 protein resides in a P-granule microenvironment devoid of assembled large and small ribosome subunits. To test whether P granules and ribosomal proteins occupy different domains in the *C. elegans* germline, GLH-1::GFP::3xFLAG germlines were costained with an antibody against RPL-7a and imaged through a single section (Figure 7A). While the RPL-7a signal was strongest in the rachis as opposed to the germline perimeter where P granules are more prevalent, this ribosomal protein is not excluded from P granules. It was previously shown that P granules extend the size exclusion properties within the nuclear pore out into the germline cytoplasm, and while fluorescent dextran molecules < 40 kDa in size diffuse freely through P granules, 70 and 155 kDa dextran molecules do not (Updike *et al.* 2011). The size of RPL-7a, estimated at 30 kDa, may allow the protein to diffuse through P granules and into the nucleus, where it can be assembled into the large ribosomal subunit. To get a better idea of whether assembled ribosomes are excluded from P granules, 18S rRNA probes were used as a proxy to visualize areas of the cytoplasm occupied by 40S subunits. 18S rRNA undergoes rapid assembly with ribosomal proteins and is exported into the cytoplasm as the 40S subunit. Previous fluorescence detection of 5S, 5.8S, 18S, and 26S rRNA probes did not show any obvious concentration of rRNA in P granules (Schisa *et al.* 2001). Stellaris smFISH probes were designed for the 18S *rrn-1.1*. The vast abundance of this rRNA causes the probe to light up the dissected germlines,

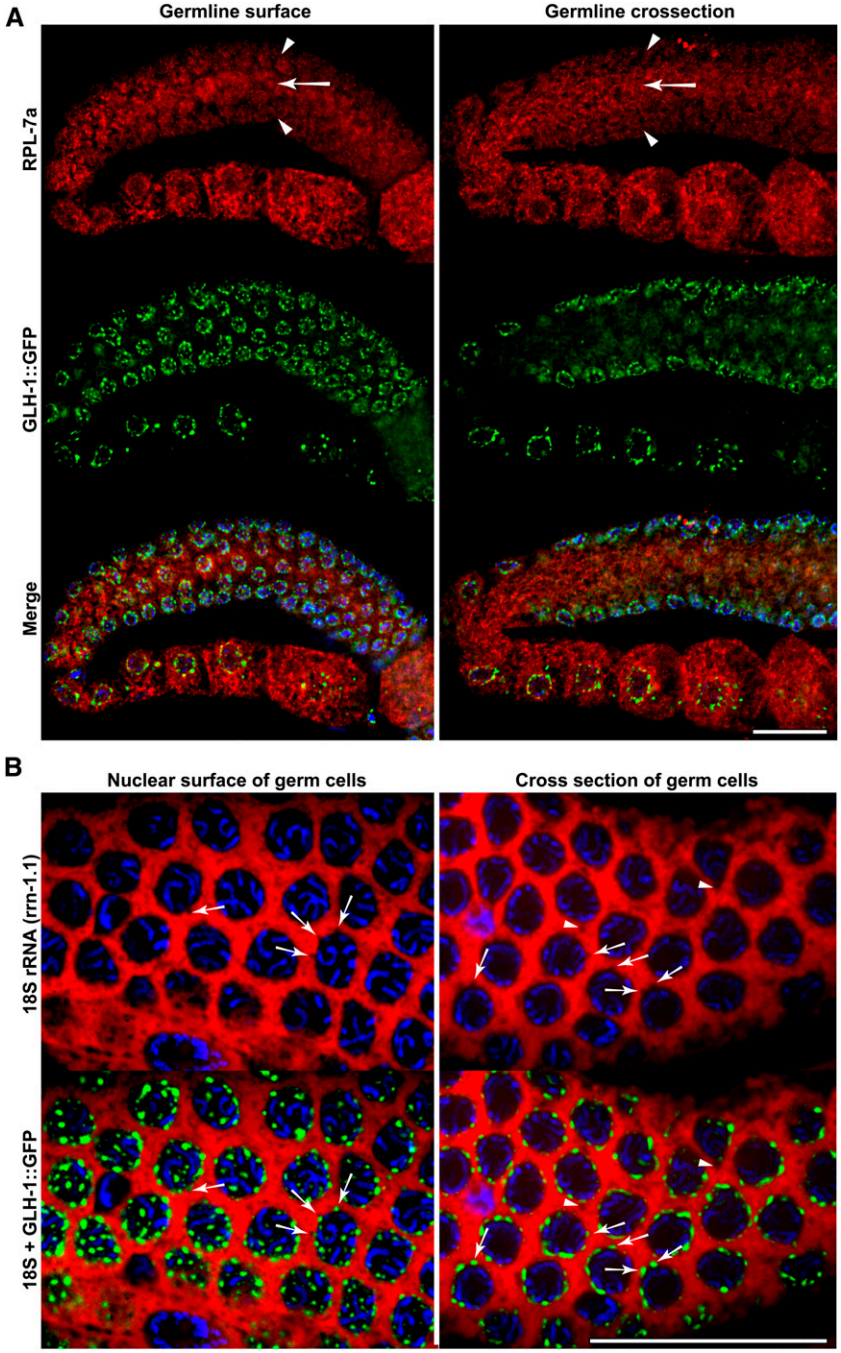

Figure 7 Ribosomes and the size exclusion properties of P granules. (A) Immunostaining of RPL-7a (red) with GLH-1::GFP. RPL-7a is more concentrated in the shared cytoplasm of the rachis (arrows) than germ granule-rich areas at the perimeter (arrowheads), but it is not excluded from P granules. (B) 18S rRNA FISH signal (red) is saturated in the cytoplasm of germ cells where it associates with the 40S ribosomal subunit, but is excluded from GLH-1::GFP-marked P (arrows) and yolk granules (arrowheads).

but voids in the cytoplasm are evident in areas occupied by GLH-1::GFP (Figure 7B). These results suggest that while some individual ribosomal proteins colocalize with P granules, assembled ribosomes do not, supporting a model where P granules partition the cytoplasm to create translationally silent microenvironments.

Finally, several established P-body (blue) and P-granule (red) components were examined in the context of GLH-1 association or exclusion (Figure 6, right column, Table S3). Generally, the average dispersal of P-granule components changes very little in the D**A**AD and D**Q**AD mutants. The D**Q**AD mutant has been utilized in other systems to capture factors that associate transiently in the piRNA amplifier complex (Xiol *et al.* 2014; Wenda *et al.* 2017). Proteomics data from the D**Q**AD mutant were examined to see if any proteins increased in significance and association. Only four proteins showed this up-and-to-the-right shift from wild-type (DEAD) (red arrows), and they included the Argonaute proteins CSR-1, PRG-1, C04F12.1, and WAGO-1. This increased association between GLH-1 and Argonautes suggests that nematodes have a complex similar to the piRNA transient amplifying complex described in insects and vertebrates,

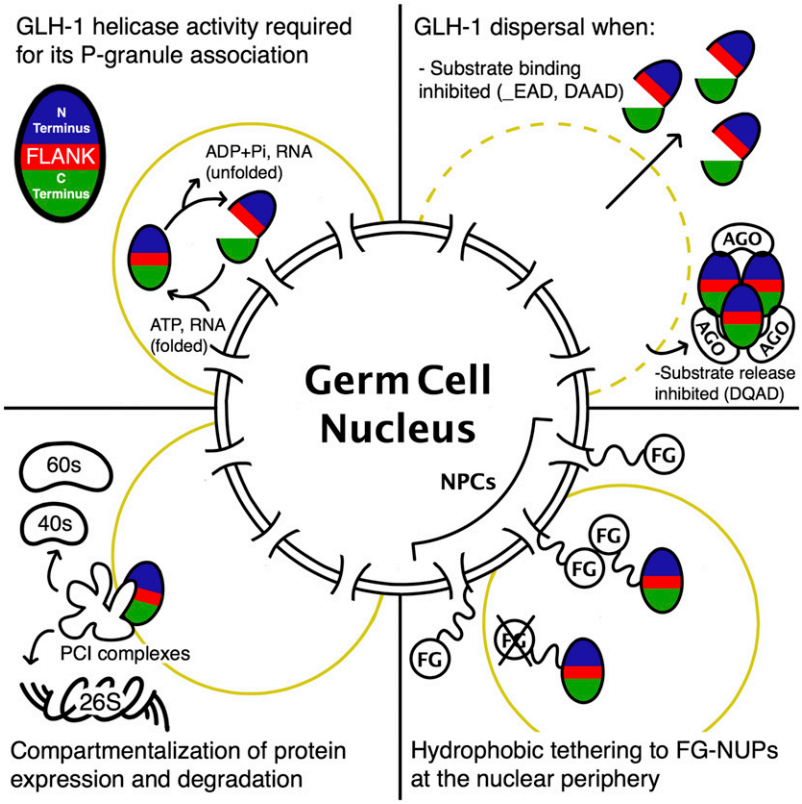

Figure 8 Summary figure. Top left; GLH-1 represented as an oval with its N-terminal (blue), flanking (red), and C-terminal helicase domains. GLH-1's association in P granules (yellow outline) requires cycles of RNA and adenosine triphosphate (ATP) binding (closed) and release of adenosine diphosphate (ADP) and phosphate (Pi). Top right; GLH-1 is dispersed in mutants that inhibit substrate binding (_EAD, DAAD) or substrate release (DQAD), and in the latter case GLH-1(DQAD) forms aggregates with specific Argonaute (AGO) proteins. Bottom left; GLH-1 associates with the PCI complexes (26S Proteasome Lid, COP9, and eIF3) while excluding ribosomal subunits (60S and 40S) and the 26S proteasome. Bottom right; The phenylalanine - glycine (FG) repeats of GLH-1 tether P granules to FG-nucleoporin proteins.

albeit one that functions through RdRPs instead of ping-pong amplification.

Discussion

The role of germ granules in inducing or maintaining germ cell potency may come down to the molecular functions of their individual components. In this study, a comparative structure–function analysis was performed on the *C. elegans* Vasa homologs. These results show that GLH-1's helicase activity is necessary to maintain its tight association with P granules (Figure 8). Every edit of a conserved residue within the helicase domains caused GLH-1 to detach from P granules and disperse into the cytoplasm. Flanking domain mutations phenocopy this dispersal, suggesting that the flanking domain facilitates this helicase activity as it wraps between the N- and C-terminal RecA domains. Whether this means that GLH-1 localization is mediated through continuous unwinding of RNA substrates or continuous cycling of other protein interactions is unclear. However, GLH-1's P-granule association is not mediated by its glycine-rich intrinsically disordered region (IDR), zinc-knuckle, negatively charged C-terminus or any inherent structural features on their own. Interestingly, while mutations in these domains do not disperse GLH-1 protein, they still exhibit close to the same degree of fertility defects at the restrictive temperature as the *glh-1* deletion, demonstrating one reason why these Vasa-defining domains have been conserved throughout evolution. The specific contribution of each of these domains will need to be ascertained through complimentary approaches that include: (1) generating similar edits and deletions in paralogs to observe additive effects, as was done with the FG-repeat deletion in GLH-1 and GLH-2, and (2) by GLH-1 IP and LC-MS/MS in these mutant strains to determine which protein enrichments are lost, and to find candidates to test for direct GLH-1 domain interactions.

One outstanding question is whether GLH-1 and P granules demonstrate an affinity to specific germline-expressed transcripts. Multiple attempts to immunoprecipitate and sequence RNA substrates of GLH-1 and PGL-1 under varying conditions have been performed by our group; however, follow-up single-molecule FISH studies have not demonstrated consistent P-granule enrichment of these identified substrates. These negative results likely reflect the nonsequence-specific and transient manner in which core P-granule components—like PGL-1 and GLH-1—interact with RNA, and they add weight to the idea that GLH-1 and Vasa proteins simply function as mRNA solvents in phase-separated P granules (Nott *et al.* 2016). This may eventually be resolved as RNA immunoprecipitation (RIP), crosslinking immunoprecipitation (CLIP)-seq technologies improve, or the right P-granule target protein is found, but the idea that P granules contain solvents to keep transcripts unfolded and accessible for sequence scanning by small RNA-bound Argonautes or other RNA-binding proteins is highly likely.

Dominant phenotypes were observed in R328Q and D554A mutations thought to uncouple ATP hydrolysis from RNA unwinding, which are possibly caused by increased energy expenditure that is not translated into enzymatic helicase activity. The D**Q**AD mutation is also dominant, but the D**A**AD mutation is not. This E to Q change may induce sterility because it accumulates large aggregates that sequester components from their normal function within P granules, or because they fail to dissolve in the soma. Since these aggregates persist in somatic blastomeres, the extent to which they resemble P granules or retain normal P-granule function is unclear. Therefore, caution should be maintained when interpreting whether D**Q**AD aggregates are capturing a transient amplifying complex or a novel aggregate altogether. Given that these dominant alleles are suppressed with an intragenic T546A mutation, they are likely anti- or neomorphic alleles. Another unreported deletion of ER residues in motif V (Vasa position 550–551) caused a stronger dominant phenotype that could not be maintained beyond two generations, suggesting that some dominant *glh-1* alleles are too severe to recover with the current approach.

With the caveats of the GLH-1(D**Q**AD) in mind, significant increases in association with this mutant were primarily restricted to Argonaute proteins. These included not only the piRNA Argonaute PRG-1, but also the Argonautes CSR-1, WAGO-1, and C04F12.1, which bind to other small RNA species. In this regard, GLH-1(D**Q**AD) reflects the transient state of its insect and mammalian homologs that interact with piRNA-amplifying Argonaute proteins, but suggests that the *C. elegans* transient complex is not limited to interactions with piRNAs. It is worth noting that the GLH-1 enriched proteins showing the most significant *decrease* in association with D**Q**AD are the PP2A subunits (PAA-1, PPTR-1, PPTR-2, and LET-92), whose phosphatase activities stabilize P granules in the early embryo (Updike and Strome 2009; Gallo *et al.* 2010; Griffin *et al.* 2011; Wang *et al.* 2014; Tables S2 and S3). This suggests that the targets of this phosphatase activity are not enriched in these D**Q**AD aggregates, and by extension may associate with GLH-1 in its open configuration but not this closed transient state.

Another exciting finding from this study is the enrichment of PCI complex zomes in the GLH-1 IPs. While GLH-1's direct association with the COP9 signalosome component CSN5 had been previously established, finding an enrichment for almost every PCI protein strongly suggests that GLH-1 has an affinity for these multilobed and structurally conserved scaffolding complexes. It will be imperative to understand how these scaffolds associate with GLH-1, the specific complex components that show direct interactions like CSN5, and whether there is a spatiotemporal element to these interactions during germline development. Interestingly, while CSN5 is found in the cytoplasm and nucleus, it exhibits no distinct P-granule enrichment (Smith *et al.* 2002; Pintard *et al.* 2003), nor have other PCI subunits to date. One model is that COP9 and the 26S Lid complex associate with GLH-1 in P granules. Another model is that, like ribosomes, assembled PCI complexes are also excluded from P granules, but facilitate the exchange of transcripts and proteins at the interface of the P-granule microenvironment to deliver them to assembled ribosomes or 26S proteasomes, respectively (Figure 8). Subsequent studies will need to determine where the interactions between PCI complex components and GLH-1 take place, whether the association between GLH-1 and the eIF3 complex mediates a positive or negative effect on translation, and the impact of GLHs on protein turnover and translational regulation.

Acknowledgments

We would like to thank Chris Smith in the Mount Desert Island Biological Laboratory (MDIBL) Sequencing Core for her assistance in sequencing and genotyping strains generated for this publication; Dorothy Wheatcraft at the mass spectrometry facility at the Jackson Laboratory for proteomics assistance and advice; Matt Stokes at Cell Signaling Technologies, Inc. for performing the proteomics and analysis of our GLH-1 IPs; Jarod Rollins at the MDIBL for ribosome antibodies; and Tai Montgomery at Colorado State University for providing small RNA-based protocols. The Updike laboratory is supported by the National Institutes of Health (NIH)-National Institute of General Medical Sciences (NIGMS) (R01 GM-113933). E.A.M. is supported by a postdoctoral National Research Service Award fellowship from the NIH-NIGMS (F32 GM-128248). Equipment and cores used for parts of this study are supported by the NIH-NIGMS Centers of Biomedical Research Excellence (P20 GM-104318) and the IDeA Networks of Biomedical Research Excellence (P20 GM-203423). Undergraduate support included a National Science Foundation-Research Experiences for Undergraduates (DBI-1460495) fellowship to J.H.F. and MDIBL's James Slater Murphy fellowship to E.L.X. The authors have no competing interests to disclose.

Literature Cited

Andralojc, K. M., A. C. Campbell, A. L. Kelly, M. Terrey, P. C. Tanner *et al.*, 2017 ELLI-1, a novel germline protein, modulates RNAi activity and P-granule accumulation in Caenorhabditis elegans. PLoS Genet. 13: e1006611. https://doi.org/10.1371/journal.pgen.1006611

Brenner, S., 1974 The genetics of Caenorhabditis elegans. Genetics 77: 71–94.

Campbell, A. C., and D. L. Updike, 2015 CSR-1 and P granules suppress sperm-specific transcription in the C. elegans germline. Development 142: 1745–1755. https://doi.org/10.1242/dev.121434

Carrera, P., O. Johnstone, A. Nakamura, J. Casanova, H. Jäckle *et al.*, 2000 VASA mediates translation through interaction with a Drosophila yIF2 homolog. Mol. Cell 5: 181–187. https://doi.org/10.1016/S1097-2765(00)80414-1

Cruciat, C.-M., C. Dolde, R. E. A. de Groot, B. Ohkawara, C. Reinhard *et al.*, 2013 RNA helicase DDX3 is a regulatory subunit of casein kinase 1 in Wnt-β-catenin signaling. Science 339: 1436–1441. https://doi.org/10.1126/science.1231499

Dehghani, M., and P. Lasko, 2015 In vivo mapping of the functional regions of the DEAD-box helicase Vasa. Biol. Open 4: 450–462. https://doi.org/10.1242/bio.201410579

Dehghani, M., and P. Lasko, 2016 C-terminal residues specific to Vasa among DEAD-box helicases are required for its functions in piRNA biogenesis and embryonic patterning. Dev. Genes Evol. 226: 401–412. https://doi.org/10.1007/s00427-016-0560-5

DeRenzo, C., K. J. Reese, and G. Seydoux, 2003 Exclusion of germ plasm proteins from somatic lineages by cullin-dependent degradation. Nature 424: 685–689. https://doi.org/10.1038/nature01887

Dickinson, D. J., A. M. Pani, J. K. Heppert, C. D. Higgins, and B. Goldstein, 2015 Streamlined genome engineering with a self-excising drug selection cassette. Genetics 200: 1035–1049. https://doi.org/10.1534/genetics.115.178335

Eng, J. K., A. L. McCormack, and J. R. Yates, 1994 An approach to correlate tandem mass spectral data of peptides with amino acid sequences in a protein database. J. Am. Soc. Mass Spectrom. 5: 976–989. https://doi.org/10.1016/1044-0305(94)80016-2

Gallo, C. M., J. T. Wang, F. Motegi, and G. Seydoux, 2010 Cytoplasmic partitioning of P granule components is not required to specify the germline in C. elegans. Science 330: 1685–1689. https://doi.org/10.1126/science.1193697

Gao, G., F. Deeb, J. M. Mercurio, A. Parfenova, P. A. Smith *et al.*, 2012 PAN-1, a P-granule component important for C. elegans fertility, has dual roles in the germline and soma. Dev. Biol. 364: 202–213. https://doi.org/10.1016/j.ydbio.2012.02.006

Griffin, E. E., D. J. Odde, and G. Seydoux, 2011 Regulation of the MEX-5 gradient by a spatially segregated kinase/phosphatase cycle. Cell 146: 955–968. https://doi.org/10.1016/j.cell.2011.08.012

Gruidl, M. E., P. A. Smith, K. A. Kuznicki, J. S. McCrone, J. Kirchner *et al.*, 1996 Multiple potential germ-line helicases are components of the germ-line-specific P granules of *Caenorhabditis elegans*. Proc. Natl. Acad. Sci. USA 93: 13837–13842. https://doi.org/10.1073/pnas.93.24.13837

Gustafson, E. A., and G. M. Wessel, 2010 Vasa genes: emerging roles in the germ line and in multipotent cells. Bioessays 32: 626–637. https://doi.org/10.1002/bies.201000001

Hanazawa, M., M. Yonetani, and A. Sugimoto, 2011 PGL proteins self associate and bind RNPs to mediate germ granule assembly in C. elegans. J. Cell Biol. 192: 929–937. https://doi.org/10.1083/jcb.201010106

Hay, B., L. Y. Jan, and Y. N. Jan, 1988 A protein component of Drosophila polar granules is encoded by vasa and has extensive sequence similarity to ATP-dependent helicases. Cell 55: 577–587. https://doi.org/10.1016/0092-8674(88)90216-4

Hubert, A., and P. Anderson, 2009 The C. elegans sex determination gene laf-1 encodes a putative DEAD-box RNA helicase. Dev. Biol. 330: 358–367. https://doi.org/10.1016/j.ydbio.2009.04.003

Ji, N., and A. van Oudenaarden, 2012 Single molecule fluorescent in situ hybridization (smFISH) of C. elegans worms and embryos (December 13, 2012), *WormBook*, ed. The C. elegans Research Community, WormBook, doi/10.1895/wormbook.1.153.1, http://www.wormbook.org. https://doi.org/10.1895/wormbook.1.153.1

Johnstone, O., and P. Lasko, 2004 Interaction with eIF5B is essential for Vasa function during development. Development 131: 4167–4178. https://doi.org/10.1242/dev.01286

Kawasaki, I., A. Amiri, Y. Fan, N. Meyer, S. Dunkelbarger *et al.*, 2004 The PGL family proteins associate with germ granules and function redundantly in Caenorhabditis elegans germline development. Genetics 167: 645–661. https://doi.org/10.1534/genetics.103.023093

Knutson, A. K., T. Egelhofer, A. Rechtsteiner, and S. Strome, 2017 Germ granules prevent accumulation of somatic transcripts in the adult Caenorhabditis elegans germline. Genetics 206: 163–178. https://doi.org/10.1534/genetics.116.198549

Kugler, J.-M., J.-S. Woo, B.-H. Oh, and P. Lasko, 2010 Regulation of Drosophila vasa in vivo through paralogous cullin-RING E3 ligase specificity receptors. Mol. Cell. Biol. 30: 1769–1782. https://doi.org/10.1128/MCB.01100-09

Kuramochi-Miyagawa, S., T. Watanabe, K. Gotoh, K. Takamatsu, S. Chuma *et al.*, 2010 MVH in piRNA processing and gene silencing of retrotransposons. Genes Dev. 24: 887–892. https://doi.org/10.1101/gad.1902110

Kutscher, L. M., and S. Shaham, 2014 Forward and reverse mutagenesis in *C. elegans* (January 17, 2014), *WormBook*, ed. The C. elegans Research Community, WormBook, doi/10.1895/wormbook.1.167.1, http://www.wormbook.org. https://doi.org/10.1895/wormbook.1.167.1

Kuznicki, K. A., P. A. Smith, W. M. Leung-Chiu, A. O. Estevez, H. C. Scott *et al.*, 2000 Combinatorial RNA interference indicates GLH-4 can compensate for GLH-1; these two P granule components are critical for fertility in C. elegans. Development 127: 2907–2916.

Lasko, P., 2013 The DEAD-box helicase Vasa: evidence for a multiplicity of functions in RNA processes and developmental biology. Biochim. Biophys. Acta. Gene Regul. Mech. 1829: 810–816. https://doi.org/10.1016/j.bbagrm.2013.04.005

Lasko, P. F., and M. Ashburner, 1988 The product of the Drosophila gene vasa is very similar to eukaryotic initiation factor-4A. Nature 335: 611–617. https://doi.org/10.1038/335611a0

Li, P., L. Xie, Y. Gu, J. Li, and J. Xie, 2017 Roles of multifunctional COP9 signalosome complex in cell fate and implications for drug discovery. J. Cell. Physiol. 232: 1246–1253. https://doi.org/10.1002/jcp.25696

Liu, N., H. Han, and P. Lasko, 2009 Vasa promotes *Drosophila* germline stem cell differentiation by activating *mei-P26* translation by directly interacting with a (U)-rich motif in its 3′UTR. Genes Dev. 23: 2742–2752. https://doi.org/10.1101/gad.1820709

Malone, C. D., J. Brennecke, M. Dus, A. Stark, W. R. McCombie *et al.*, 2009 Specialized piRNA pathways act in germline and somatic tissues of the Drosophila ovary. Cell 137: 522–535. https://doi.org/10.1016/j.cell.2009.03.040

Marnik, E. A., and D. L. Updike, 2019 Membraneless organelles: P granules in Caenorhabditis elegans. Traffic 20: 373–379. https://doi.org/10.1111/tra.12644

Megosh, H. B., D. N. Cox, C. Campbell, and H. Lin, 2006 The role of PIWI and the miRNA machinery in Drosophila germline determination. Curr. Biol. 16: 1884–1894. https://doi.org/10.1016/j.cub.2006.08.051

Meister, C., M. K. Gulko, A. M. Köhler, and G. H. Braus, 2016 The devil is in the details: comparison between COP9 signalosome (CSN) and the LID of the 26S proteasome. Curr. Genet. 62: 129–136. https://doi.org/10.1007/s00294-015-0525-7

Nott, T. J., E. Petsalaki, P. Farber, D. Jervis, E. Fussner *et al.*, 2015 Phase transition of a disordered nuage protein generates environmentally responsive membraneless organelles. Mol. Cell 57: 936–947. https://doi.org/10.1016/j.molcel.2015.01.013

Nott, T. J., T. D. Craggs, and A. J. Baldwin, 2016 Membraneless organelles can melt nucleic acid duplexes and act as biomolecular filters. Nat. Chem. 8: 569–575. https://doi.org/10.1038/nchem.2519

Oldenbroek, M., S. M. Robertson, T. Guven-Ozkan, S. Gore, Y. Nishi *et al.*, 2012 Multiple RNA-binding proteins function combinatorially to control the soma-restricted expression pattern of the E3 ligase subunit ZIF-1. Dev. Biol. 363: 388–398. https://doi.org/10.1016/j.ydbio.2012.01.002

Orsborn, A. M., W. Li, T. J. McEwen, T. Mizuno, E. Kuzmin *et al.*, 2007 GLH-1, the C. elegans P granule protein, is controlled by the JNK KGB-1 and by the COP9 subunit CSN-5. Development 134: 3383–3392. https://doi.org/10.1242/dev.005181

Paix, A., A. Folkmann, and G. Seydoux, 2017 Precision genome editing using CRISPR-Cas9 and linear repair templates in

C. elegans. Methods 121–122: 86–93. https://doi.org/10.1016/j.ymeth.2017.03.023

Pause, A., and N. Sonenberg, 1992 Mutational analysis of a DEAD box RNA helicase: the mammalian translation initiation factor eIF-4A. EMBO J. 11: 2643–2654. https://doi.org/10.1002/j.1460-2075.1992.tb05330.x

Pintard, L., T. Kurz, S. Glaser, J. H. Willis, M. Peter *et al.*, 2003 Neddylation and deneddylation of CUL-3 is required to target MEI-1/Katanin for degradation at the meiosis-to-mitosis transition in C. elegans. Curr. Biol. 13: 911–921. https://doi.org/10.1016/S0960-9822(03)00336-1

Poon, J., G. M. Wessel, and M. Yajima, 2016 An unregulated regulator: vasa expression in the development of somatic cells and in tumorigenesis. Dev. Biol. 415: 24–32. https://doi.org/10.1016/j.ydbio.2016.05.012

Schisa, J. A., J. N. Pitt, and J. R. Priess, 2001 Analysis of RNA associated with P granules in germ cells of C. elegans adults. Development 128: 1287–1298.

Sengoku, T., O. Nureki, A. Nakamura, S. Kobayashi, and S. Yokoyama, 2006 Structural basis for RNA unwinding by the DEAD-box protein Drosophila vasa. Cell 125: 287–300. https://doi.org/10.1016/j.cell.2006.01.054

Sheth, U., J. Pitt, S. Dennis, and J. R. Priess, 2010 Perinuclear P granules are the principal sites of mRNA export in adult C. elegans germ cells. Development 137: 1305–1314. https://doi.org/10.1242/dev.044255

Shirayama, M., W. Stanney, W. Gu, M. Seth, and C. C. Mello, 2014 The Vasa homolog RDE-12 engages target mRNA and multiple argonaute proteins to promote RNAi in C. elegans. Curr. Biol. 24: 845–851. https://doi.org/10.1016/j.cub.2014.03.008

Smith, P., W.-M. Leung-Chiu, R. Montgomery, A. Orsborn, K. Kuznicki *et al.*, 2002 The GLH proteins, Caenorhabditis elegans P granule components, associate with CSN-5 and KGB-1, proteins necessary for fertility, and with ZYX-1, a predicted cytoskeletal protein. Dev. Biol. 251: 333–347. https://doi.org/10.1006/dbio.2002.0832

Spike, C., N. Meyer, E. Racen, A. Orsborn, J. Kirchner *et al.*, 2008 Genetic analysis of the Caenorhabditis elegans GLH family of P-granule proteins. Genetics 178: 1973–1987. https://doi.org/10.1534/genetics.107.083469

Strome, S., and D. Updike, 2015 Specifying and protecting germ cell fate. Nat. Rev. Mol. Cell Biol. 16: 406–416. https://doi.org/10.1038/nrm4009

Updike, D. L., and S. Strome, 2009 A genomewide RNAi screen for genes that affect the stability, distribution and function of P granules in Caenorhabditis elegans. Genetics 183: 1397–1419. https://doi.org/10.1534/genetics.109.110171

Updike, D. L., S. J. Hachey, J. Kreher, and S. Strome, 2011 P granules extend the nuclear pore complex environment in the C. elegans germ line. J. Cell Biol. 192: 939–948. https://doi.org/10.1083/jcb.201010104

Updike, D. L., A. K. Knutson, T. A. Egelhofer, A. C. Campbell, and S. Strome, 2014 Germ-granule components prevent somatic development in the C. elegans germline. Curr. Biol. 24: 970–975. https://doi.org/10.1016/j.cub.2014.03.015

Voronina, E., and G. Seydoux, 2010 The C. elegans homolog of nucleoporin Nup98 is required for the integrity and function of germline P granules. Development 137: 1441–1450. https://doi.org/10.1242/dev.047654

Wang, J. T., J. Smith, B.-C. Chen, H. Schmidt, D. Rasoloson *et al.*, 2014 Regulation of RNA granule dynamics by phosphorylation of serine-rich, intrinsically disordered proteins in C. elegans. Elife 3: e04591. https://doi.org/10.7554/eLife.04591

Wenda, J. M., D. Homolka, Z. Yang, P. Spinelli, R. Sachidanandam *et al.*, 2017 Distinct roles of RNA helicases MVH and TDRD9 in PIWI slicing-triggered mammalian piRNA biogenesis and function. Dev. Cell 41: 623–637.e9. https://doi.org/10.1016/j.devcel.2017.05.021

Xiol, J., P. Spinelli, M. Laussmann, D. Homolka, Z. Yang *et al.*, 2014 RNA clamping by Vasa assembles a piRNA amplifier complex on transposon transcripts. Cell 157: 1698–1711. https://doi.org/10.1016/j.cell.2014.05.018

Yang, H., J. Vallandingham, P. Shiu, H. Li, C. P. Hunter *et al.*, 2014 The DEAD box helicase RDE-12 promotes amplification of RNAi in cytoplasmic foci in C. Elegans. Curr. Biol. 24: 832–838. https://doi.org/10.1016/j.cub.2014.01.008

Communicating editor: S. Kennedy